CHEMISTRY
A EUROPEAN JOURNAL

DOI: 10.1002/chem.200601278

Comparative Experimental and EXAFS Studies in the Mizoroki–Heck Reaction with Heteroatom-Functionalised N-Heterocyclic Carbene Palladium Catalysts

Steven G. Fiddy,*[b, d] John Evans,[a, c] Thomas Neisius,[d] Mark A. Newton,[d] Nikolaos Tsoureas,[a] Arran A. D. Tulloch,[a] and Andreas A. Danopoulos*[a]

Abstract: A study on the Mizoroki–Heck coupling of selected aryl bromides with acrylates catalysed by a series of Pd complexes of bidentate pyridyl-, picolyl-, diphenylphosphinoethyl- and diphenylphosphinomethyl-functionalised N-heterocyclic carbene (NHC) is reported. The observed activity is dependent on the type of solvent and base used and the nature of the "classical" donors of the mixed-donor bidentate ligand and its bite angle. A mechanistic model is presented for the pyridine-functionalised NHC complexes based on an in situ EXAFS study under dilute catalyst conditions (2 mM Pd). The model involves pre-dissociation of the pyridine functionality and oxidative addition of ArBr in the early stages of the reaction, as well as formation of monomeric and dimeric Pd species at the time of substrate conversion.

Keywords: carbene ligands · EXAFS spectroscopy · Heck reaction · homogeneous catalysis · palladium

Introduction

Research into the discovery of new catalysts for C–C bond formation has given active systems for Suzuki–Miyaura, Kumada and Negishi coupling, even with unreactive aryl chlorides as substrates.[1] Some of the successful catalysts are formed by a combination of Pd^0 precursors and trialkylphosphines, phosphites, N-heterocyclic carbenes (NHCs) and palladacycles which generate the catalytic species in situ.[2] Well-defined Pd^0 complexes have also been used for this purpose with variable activity, occasionally inferior to systems formed in situ. In contrast, the development of catalysts for the Mizoroki–Heck reaction has proceeded at a slower pace. In particular, the general coupling of aryl chlorides with alkenes under mild conditions has still not been realised. In addition, many questions on the mechanism of catalysis remain unanswered, including the nature of the active species, the involvement of palladium nanoparticles, the role of the halide ions as ligands and so on.[3] Palladium complexes with simple monodentate or bidentate NHC ligands, either pre-formed or generated in situ from imidazolium salts and palladium acetate, were first introduced as Mizoroki–Heck catalysts by Herrmann et al.[4] Catalysts formed from Pd^{II} and mixed-donor bidentate ligands with NHC and phosphine donors were predicted to be superior catalysts[5] by virtue of the hemilability of the phosphine donor of the heterobifunctional ligand system. Preliminary experimental data did not confirm this prediction, even though the catalysts showed good activity with aryl bromides, while they were inactive with aryl chlorides.[6] Catalysts formed from Pd^{II} and bidentate ligands with mixed NHC and pyridine donors showed high activity with aryl iodides and bromides as substrates under high dilution, but conversions with unactivated or deactivated aryl chlorides was low even under

[a] Prof. J. Evans, Dr. N. Tsoureas, Dr. A. A. D. Tulloch, Dr. A. A. Danopoulos
School of Chemistry
University of Southampton
Highfield, Southampton, SO17 1BJ (UK)
Fax: (+44) 238-059-6805
E-mail: ad1@soton.ac.uk

[b] Dr. S. G. Fiddy
CCLRC Daresbury Laboratory
Warrington, WA4 4AD (UK)
Fax: (+44) 192-560-3124
E-mail: s.g.fiddy@dl.ac.uk

[c] Prof. J. Evans
Diamond Light Source, Chilton, OX11 0DE (UK)

[d] Dr. S. G. Fiddy, Dr. T. Neisius, Dr. M. A. Newton
The European Synchrotron Radiation Facility
6 rue Jules Horowitz, BP220, 38043 Grenoble (France)

Supporting information for this article is available on the WWW under http://www.chemeurj.org/ or from the author.

harsh conditions.[7] The potential hemilability of the pyridine donor of the bidentate ligand has been considered as a possible reason for the observed high activity, even though direct evidence (mainly spectroscopic) of its occurrence was difficult to obtain. Recently, a few reports claimed that, as a consequence of the forcing reaction conditions employed in the high-temperature Mizoroki–Heck reaction, the catalytic species responsible for the transformation are Pd nanoparticles rather than metal complexes operating in solution.[3]

Here we compare the activity in the Mizoroki–Heck reaction of functionalised NHC complexes of Pd that we have recently prepared (Scheme 1).[7a,8,9]

We also describe efforts to probe the nature of the dissolved species in a catalytic solution obtained from **2c** or **2d** using EXAFS in solution.

Results and Discussion

Selected catalytic data for the Mizoroki–Heck reaction of phenyl bromides are given in Tables 1 and 2. All of the complexes catalyse the coupling of activated and unactivated aryl bromides with electron-deficient alkenes. Prolonged reaction times, high temperatures and low catalyst loadings under dilute conditions lead to high turnover numbers, especially with the pyridine-functionalised ligands. This manifests the good thermal stability of the active species under catalytic conditions. In all runs in which a pyridine- or picoline-functionalised NHC complex was used as catalyst precursor, there is no visible indication of Pd black formation during the reaction; however, small amounts of Pd black were observed with the phosphine-functionalised ligands. With the picoline-functionalised ligands there is no strong influence of the nature of the NHC substituents on activity. (Table 1, entries 5 versus 6 and 8 versus 9); however, over

Table 1. Comparative activity data in the coupling of various aryl bromides and acrylates catalysed by pyridine- and picoline-functionalised N-heterocyclic carbene palladium complexes. Solvent was NMP in all reactions.

Entry	Aryl halide	Alkene[a]	Cat.[b]	T [°C]	t [h]	Base	Yield [%]	TON
1	C_6H_5Br	MA	**1a**	140	18	NEt_3	20	2900
2	4-$CH_3OC_6H_4Br$	BA	**1a**	140	18	Et_3N	4	4300
3	4-$NO_2C_6H_4Br$	BA	**1a**	140	18	NaOAc	100	200
4	4-$CH_3COC_6H_4Br$	BA	**1a**	140	18	NaOAc	100	200
5	4-$CH_3COC_6H_4Br$	MA	**1a**	140	18	Et_3N	60	850
6	4-$CH_3COC_6H_4Br$	MA	**1c**	140	18	Et_3N	66	950
7	4-$CH_3COC_6H_4Br$	MA	**2c**	140	18	Et_3N	74	1050
8	C_6H_5Br	MA	**1a**	140	75	Et_3N	35	5000
9	C_6H_5Br	MA	**1c**	140	80	Et_3N	40	5700
10	C_6H_5Br	MA	**2c**	140	80	Et_3N	48	12900

[a] BA: butyl acrylate, MA: methyl acrylate. [b] Catalyst concentration was 3.5×10^{-4} M in all reactions.

Table 2. Comparative activity data for the coupling of aryl bromides with acrylates catalysed by phosphine- and pyridine-functionalised N-heterocyclic carbene palladium complexes and bis(N-heterocyclic carbene) palladium catalysts. Solvent was NMP in all reactions except for entries 17–21, for which the solvent was *N*,*N*-dimethylacetamide.

Entry	Aryl halide	Alkene[a]	Cat.[b]	T [°C]	t [h]	Base	Yield [%]	TON
1	4-$CH_3COC_6H_4Br$	MA	**3c**	120	6	NEt_3	92	185
2	4-$CH_3COC_6H_4Br$	MA	**3b**	120	6	NEt_3	67	134
3	4-$CH_3COC_6H_4Br$	MA	**4c**	120	6	NEt_3	100	200
4	4-$CH_3COC_6H_4Br$	MA	**5c**	120	6	NEt_3	100	200
5	4-$CH_3COC_6H_4Br$	MA	**3c**	120	6	Cs_2CO_3	5	10
6	4-$CH_3COC_6H_4Br$	MA	**3b**	120	6	Cs_2CO_3	55	110
7	4-$CH_3COC_6H_4Br$	MA	**4c**	120	6	Cs_2CO_3	32	65
8	4-$CH_3COC_6H_4Br$	MA	**2c**	120	6	Cs_2CO_3	100	200
9	4-$CH_3COC_6H_4Br$	MA	**5c**	120	6	Cs_2CO_3	100	200
10	C_6H_5Br	MA	**3c**	120	6	NEt_3	10	20
11	C_6H_5Br	MA	**3b**	120	6	NEt_3	22	45
12	C_6H_5Br	MA	**4c**	120	6	NEt_3	17	35
13	C_6H_5Br	MA	**2c**	120	6	NEt_3	35	70
14	C_6H_5Br	MA	**5c**	120	6	NEt_3	52	105
15	C_6H_5Br	MA	**3c**	120	6	Cs_2CO_3	16	32
16	C_6H_5Br	MA	**3b**	120	6	Cs_2CO_3	18	35
17	C_6H_5Br	MA	**3c**	120	6	Cs_2CO_3	61	122
18	C_6H_5Br	MA	**3b**	120	6	Cs_2CO_3	28	56
19	C_6H_5Br	MA	**4c**	120	6	Cs_2CO_3	90	180
20	C_6H_5Br	MA	**2c**	120	6	Cs_2CO_3	45	90
21	C_6H_5Br	MA	**5c**	120	6	Cs_2CO_3	95	190

[a] MA: methyl acrylate. [b] Catalyst concentration was 5×10^{-2} M in all reactions.

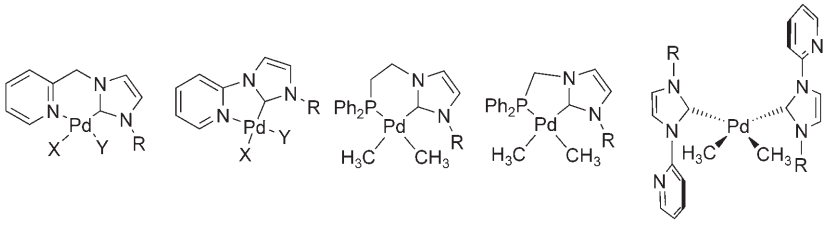

Scheme 1. Pd^{II} complexes used as catalytic precursors in the coupling of aryl bromides with acrylates. **a**: R = *t*Bu; **b**: R = mesityl; **c**: R = DiPP (Dipp = 2,6-*i*$Pr_2C_6H_3$); X = Br, OTf (only for **2d**), Y = Me.

long reaction times the pyridine-functionalised system is slightly more active than the picoline analogue (Table 1, entries 9 versus 10). Further comparison of the picoline- and pyridine-functionalised complexes is possible by plotting conversion versus reaction time (see Figure 1).

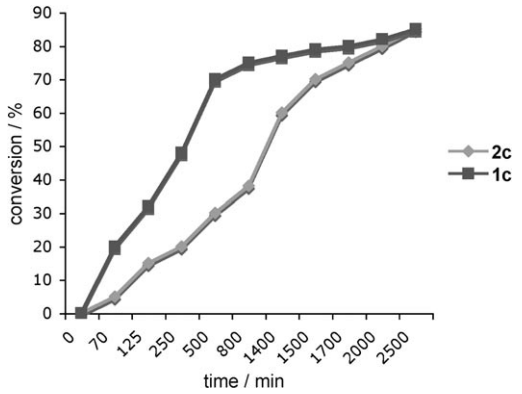

Figure 1. Comparison of the conversion of the coupling of bromoacetophenone with methyl acrylate in the presence of triethylamine with **1c** and **2c** as pre-catalysts. Amounts: Aryl bromide 5 mmol, alkene/amine 6 mmol, catalyst 3.5×10^{-4} mmol.

Interestingly, the initial rates of the system based on pre-catalyst **1c** are higher than those of **2c**. The reasons for this behaviour are not fully understood, although it may be related to different rates of the pre-activation process involving dissociation of the pyridine donor from the metal atom. This has also emerged as plausible initiation step, based on the interpretation of the solution EXAFS data (see below). Finally, the best base for the reactions described in Table 1 is triethylamine.

The activities of the phosphine-functionalised NHC complexes with five- and six-membered chelate rings and of the monodentate dicarbene complex **5c** are similar when triethylamine is used as base (Table 2, entries 1, 3 and 4). However, for the coupling of 4-bromoacetophenone, replacement of triethylamine by Cs_2CO_3 results in a drop of the activity for the systems based on the phosphine-functionalised ligands **3c** and **4c** as compared to the pyridine-functionalised **2c** and dicarbene **5c**. The activity of all catalysts for the unactivated bromobenzene is lower than for 4-bromoacetophenone, as expected. Interestingly, the activity of the phosphine-based **3c** and **4c** towards bromobenzene with Cs_2CO_3 as base is superior to that of the pyridine-based system if dimethylacetamide is used as solvent.

EXAFS studies on the pyridine-functionalised NHC palladium catalytic system: Initially, a spectrum of precatalyst **2c** in the solid state and under non-catalytic conditions (solution in *N*-methylpyrrolidone, NMP) was recorded at room temperature and compared to the crystallographic model previously published.[7a,9] This was conducted to 1) show that the EXAFS data collected in this study provide a reasonable fit to the crystallographic model and 2) discover whether any structural changes could be detected in solution under dilute conditions. Pd K-edge standard EXAFS analysis for the pure isolated complex in the solid state (Figure 2a, Table 1 in the Supporting Information) gave the expected three-shell model of a first coordination shell of two carbon atoms at 2.01 Å, a second coordination shell of one nitrogen atom at 2.21 Å and a third coordination shell of one bromine atom at 2.48 Å. Splitting of the first carbon shell into two separate shells did not lead to a significant improvement of the data. Importantly, EXAFS analysis provides proof of coordination of $N_{pyridine}$ to Pd. Although distinguishing between C and N is virtually impossible in this situation, there

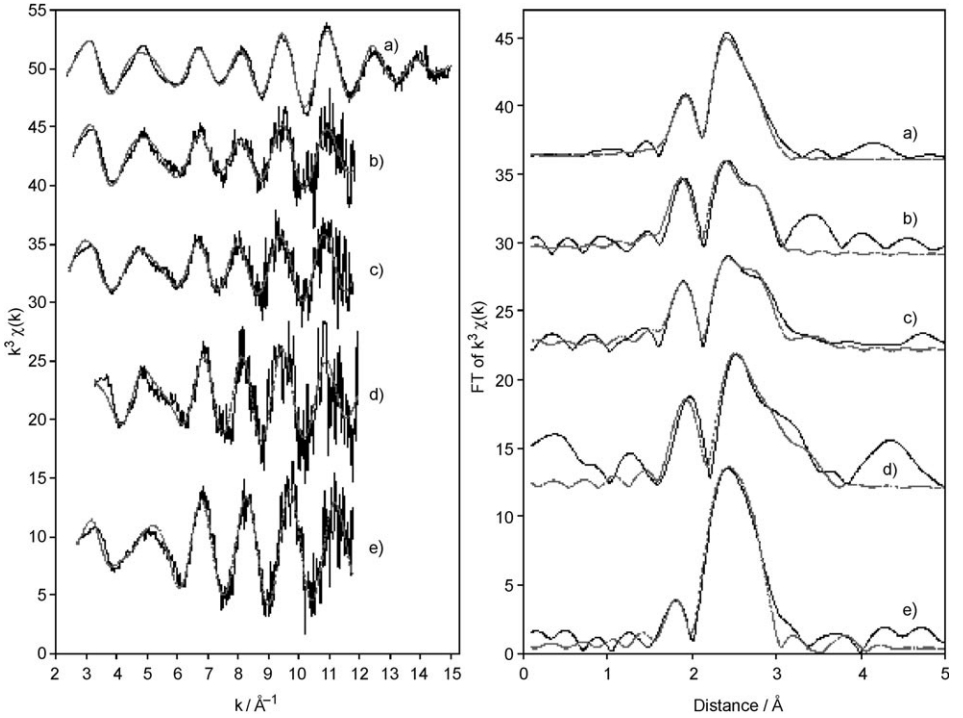

Figure 2. Pd K-edge k^3-weighted EXAFS and Fourier transform, phase-shift-corrected for carbon, of a Pd bromine carbene catalyst (**2c**, Scheme 1) a) in the solid-state form, b) 2 mM in NMP and during the Mizoroki–Heck reaction (2 mM Pd) after c) 353 K, d) 5 mins at 403 K and e) 20 mins at 403 K. Black and grey lines represent the experimental and theoretical fits derived from spherical wave analysis in EXCURV98, respectively. The time represents the total time at the reaction temperature of 403 K; however, the catalytic solution was quenched to room temperature at each of these time intervals to allow six scans to be recorded on the catalytic solution. Once this was completed, the solution was then heated back to 403 K for the required amount of time before quenching to room temperature at the next time interval.

is a good match between the Pd–$N_{pyridine}$ distance in the crystallographic data and the EXAFS model. Other distances obtained from the EXAFS analysis are also comparable to the crystallographic data[9] (in the solid the average Pd–C_{NHC}, Pd–C_{methyl}, Pd–$N_{pyridine}$ and Pd–Br distances are 1.97, 2.03, 2.17 and 2.45 Å, respectively). Furthermore, addition of a fourth shell of about one nitrogen atom at 2.87 Å decreases the *R* factor (from 26.2% to 24.3%) and improves the fit of the data. However, if the coordination number of the fourth, nitrogen shell is increased from one to two, the *R* factor increases by about 9%, which is consistent with the crystallographic model. Incorporation of the NHC functionality in a chelate ring results in unequal distances between the two N atoms of the imidazole ring and the Pd centre: the Pd–N_{NHC} distance for the N atom bonded to the pyridine moiety is significantly shorter than that for the N atom attached to the DiPP ring (2.82 Å versus 3.15 Å, respectively). Attempts were also made to incorporate extra carbon atoms to model the carbon backbone between the imidazole and pyridine rings. Evans et al.[10] showed that, in some cases, the Ni···$C_{backbone}$ carbon atoms could be detected for a series of tris(diamine) complexes, in particular for the cyclohexanediamine complexes in which the methylene carbons in the 3,6-positions were forced to be equatorial. With the present materials, detection of the carbon backbone is hypothesised to be very difficult, due to the unsymmetrical chelation and the lack of carbon atoms involved in the backbone.

Furthermore, the solid-state data reported so far were analysed in a *k* range of 2.8–15 $Å^{-1}$, but analysis of the complex dilute conditions (0.002 M Pd) in solution is only realistically possible between 2.8 and 11 $Å^{-1}$. To determine whether the smaller *k* range causes any significant problems, the solid-state data were also analysed between 2.8 and 11 $Å^{-1}$ (Table 1b in the Supporting Information). With the smaller *k* range, negative Debye–Waller factors appeared for the short-range nitrogen shell and distances varied significantly compared to the crystallographic data. However, by using k^1-weighted data (as well as k^3-weighted data) for this smaller *k* range, the parameters determined became more consistent with the crystallographic distances and therefore, for the EXAFS studies under dilute conditions, the data shown here represent parameters obtained from analysis of k^3-weighted data (but with significant consideration of the k^1-weighted data and parameters). Both forms of the weighted data provide valuable information in the analysis, as the k^1-weighted data enhance the contribution of the lighter scatterers, where as the k^3-weighted data enhance the contribution of bromine and other more distant shells of scatterers.

Ultradilute Pd K-edge EXAFS analysis of an NMP solution of complex **2c** (0.002 M Pd) at room temperature could be best fitted to a first co-ordination sphere for the carbene with about two light backscatters (C) at 2.01 Å and a second coordination sphere of one bromine atom at 2.48 Å. Also at this stage, a shell of one nitrogen atom at a distance of 2.19 Å can also be fitted successfully and significantly to both the k^1-weighted and k^3-weighted experimental data (a reduction in *R* factor of approximately 25% was observed when this extra shell was added to the k^1-weighted data). This suggests that complex **2c** is stable in solution at room temperature and the stated concentration and that $N_{pyridine}$ of the ligand remains bound even in a polar solvent. A further shell of one nitrogen could also be successfully fitted at 2.83 Å for the k^1-weighted data (2.88 Å for the k^3-weighted data), and this causes a reduction in the *R* factor. This distance is consistent with the shorter Pd–N_{NHC} distance fitted for the single-crystal data.

There is still little known about the mechanism operating with carbene-type catalysts.[3] The EXAFS spectroscopic study was intended to probe the following questions: 1) Are Pd nanoparticles formed during the reaction? 2) Is there evidence for the generation of Pd^0 by reductive elimination of 2-methylimidazolium salts from the starting precatalyst? 3) Does the pyridine arm of the bidentate ligand detach from Pd during the catalysis? 4) Is there any observable loss of bromide during the reaction which could offer an alternative possibility for alkene coordination?

Hence, ultradilute XAS studies of the Pd/carbene system were then conducted under the conditions for the coupling of *n*-butyl acrylate with *p*-bromoacetophenone in order to identify any species present during the catalytic reactions and possibly determine the structure of the catalysts in solution under dilute conditions. After a solution of complex **2c**, butyl acrylate and *p*-bromoacetophenone in NMP had been injected into the cell, it was heated gradually (10 K min^{-1}) to the reaction temperature (403 K) and, at certain intervals, the cell was rapidly cooled to 263 K to quench the reaction, thereby providing a "snapshot" of the intermediate species present in solution. The progress of the reaction was monitored under the same temperature regime by taking aliquots and analysing quantitatively the reaction mixture by gas chromatography (Figure 3).

Initially, the catalytic solution at room temperature before heating provided a structure with almost identical parameters to those observed for **2c** in the non-catalytic NMP solution, with a positive indication from the EXAFS analysis that a shell of one nitrogen atom could be incorporated to model any pyridine interaction. A second measurement was made after the catalytic solution had reached 353 K and had been quenched to room temperature. Even after heating, the Pd pre-catalyst remained intact and no significant changes in structure were seen. After cooling, EXAFS indicated that the best theoretical model of the data consisted of two carbon atoms at 2.03 Å, one nitrogen atom at 2.19 Å and one bromine atom at 2.49 Å (Table 2 in the Supporting Information). Even though the shell of nitrogen at 2.19 Å could be fitted significantly to the experimental data, the Debye–Waller factor for this shell was relatively high. Hypotheses that might explain this are that the Pd–$N_{pyridine}$ bond is weakened, and consequently the nitrogen atom is able to move with a higher degree of freedom[11] or some of the bidentate ligand acts as monodentate (cf. complex **5c**). A further shell of one nitrogen atom at 2.93 Å can also be

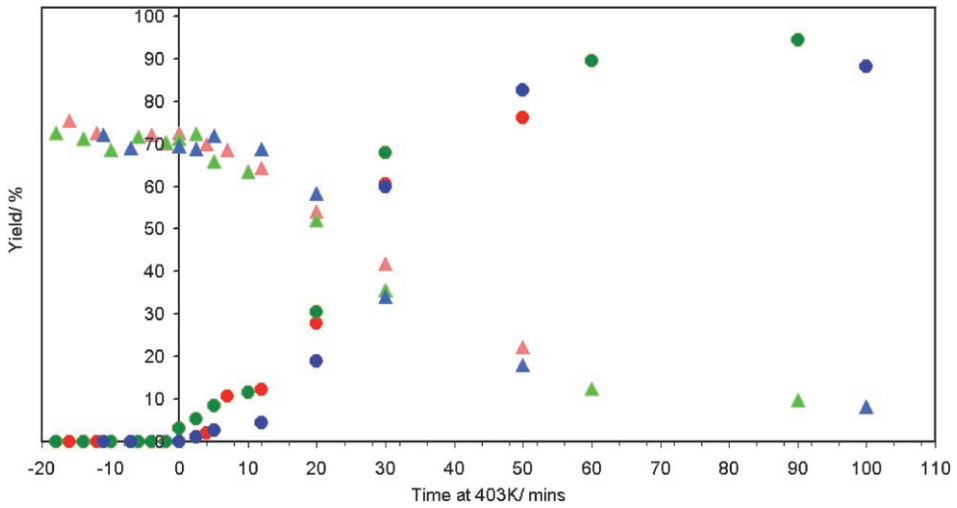

Figure 3. Reaction profile for the Mizoroki–Heck reaction between 4-bromoacetophenone and butyl acrylate. Red: pre-catalyst **2c**, green: precatalyst **2c** (repeat), blue: pre-catalyst **2d**; circles denote product, triangles denote reactant (4-bromoacetophenone); negative times represent temperature between 287 and 403 K while solution was heated at 5 K min^{-1}. Catalyst concentration = 0.002 M Pd.

added to the model, which improves the fit and decreases the *R* factor by about 7%. This nitrogen atom is proposed to be the NHC nitrogen atom, and this indicates that at this temperature the carbene ligand remains intact and bound to the Pd centre.

Refinement of the model for the experimental data of the solution that had been heated to 403 K showed a significant change (Table 2c in the Supporting Information). In this case a shell of one N atom at about 2.19 Å could not be successfully fitted for both the k^1- and k^3-weighted data and did not provide a further improvement in the fit. This is consistent with previous measurements in which the high Debye–Waller factors suggested greater lability of the pyridine nitrogen atom and/or complete loss of the Pd–$N_{pyridine}$ bond for some catalyst at 353 K. The absence of a Pd–N distance at this stage is interesting if not wholly unexpected, as the hemilabile nature of the pyridine ligand will presumably hinder detection of the pyridine N shell. It may also indicate that, at 403 K, the Pd–$N_{pyridine}$ interaction becomes labile, and possibly a co-ordination site is left free. Attempts to fit further shells to model any solvent interactions did not improve the fitting of the EXAFS data. Consequently, although no conclusive evidence can be drawn, our analysis suggests that the loss of pyridine "coordination" at this temperature may provide a free site for co-ordination of the olefin (Reaction (ii), Scheme 2) before insertion into the Pd–C σ bond. Analysis of the longer Pd–N distance also provides further indirect evidence that complete dissociation of the pyridine functional group from the Pd centre may occur. The analysis can be best fitted now to a shell of two nitrogen atoms at 2.90 Å, consistent with dissociation of the pyridyl group and the ligand acting as monodentate from the NHC end (see structures **10**–**12** in ref. [9] or complex **5c** in this paper).

After a further 5 min at 403 K (and subsequent quenching to room temperature), another significant change was noted: addition of a shell of one palladium atom at 2.74 Å improved the *R* factor and provided a better fit to the Fourier transform; attempts to fit more than one palladium atom

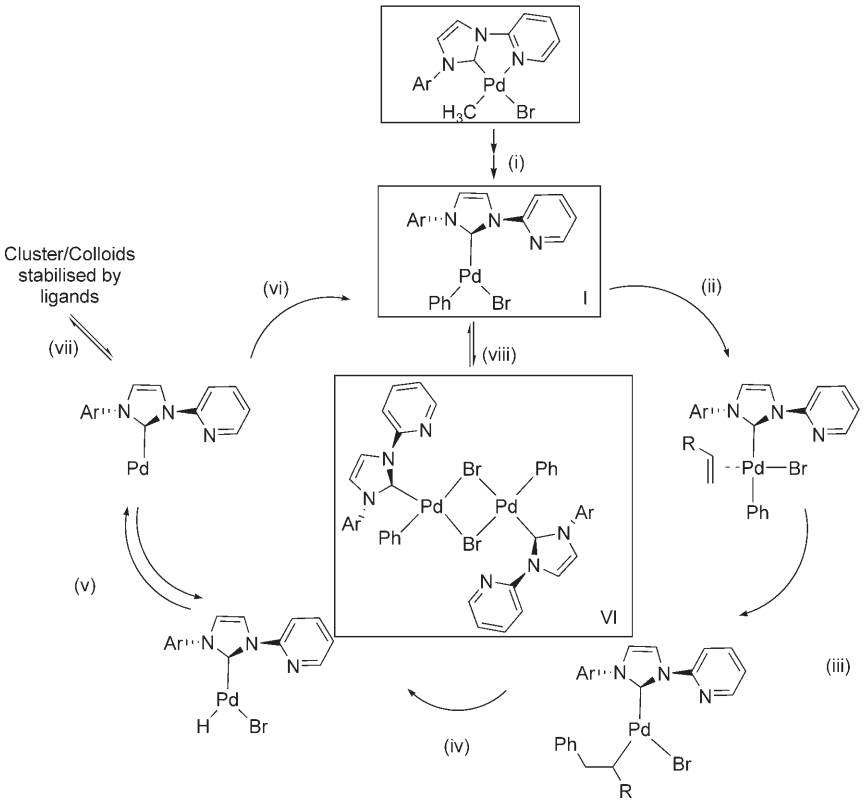

Scheme 2. Proposed mechanism for the Mizoroki–Heck reaction of bromoacetophenone with butyl acrylate catalysed by **2c** (observed species characterised by XAS indicated by boxes; the remainder are all plausible transient species).

to the data led only to deterioration in the fit. This points to several possibilities: 1) Br-bridged dimer species were formed (this is thought to be highly unlikely, as the Pd–Pd distance is too short in comparison with those observed for bromine-bridged palladium dimers, which range from 3.50 to 3.75 Å),[12] 2) direct Pd–Pd dimers and trimers are formed,[13] 3) small soluble colloidal particles are formed, either by loss of the NHC ligand (as imidazolium) or by loss of HBr and stabilisation of the colloids towards formation of Pd black by the NHC ligands (reaction (vii), Scheme 2) or 4) a small percentage of the palladium has been converted to large palladium particles or "Pd black". However, if the last possibility is correct, the Pd–Pd interaction must be caused by a small percentage of these large particles due to the low coordination number of the palladium shell. For example, for a fcc spherical Pd particle (diameter ca. 40 Å) consisting of about 2171 atoms, the first shell coordination number from XAS would be approximately 10.[14] However, as the Pd–Pd coordination number observed for this model was only 1, it means that only about 10% of the palladium could be in the form of large palladium particles. In combination with the appearance of a palladium interaction in the EXAFS data, it is also noted that the yield of product is low at this stage and the reaction profile appears to show an induction period in the reaction, which could be related to the formation of these soluble Pd colloids.

Moreover, after a further 5 min at 403 K (10 min total time at 403 K), the best theoretical model that could be fitted to the experimental EXAFS data does not contain a Pd shell. The best fit to the data consists of a simple two-shell model of two carbon atoms at 2.04 Å and one bromine atom at 2.49 Å. When a shell of palladium is fitted, the *R* factor does not decrease at all. At this stage, it is unclear why the shell of palladium would appear then disappear. Possible hypotheses include: 1) rapid conversion of the dimeric and trimeric species (which are initially formed) to monomeric species when excess Br^- becomes available or 2) conversion of palladium colloids to the catalytically active monomeric or possibly dimeric species. This is consistent with the findings of De Vries[3b] that monomeric and dimeric species (which are the active species in the mechanism proposed) are formed from stabilised Pd nanoparticles. However, if a shell of two nitrogen atoms is added at a distance of 2.88 Å, the significant reduction in the *R* factor suggests that the carbene ligand remains attached to a large majority of the palladium at this stage of the reaction, probably either stabilising the Pd against Pd black formation or as one of the intermediates in the proposed mechanism, that is, the product of oxidative addition (note: when a shell of one nitrogen atom is added, negative Debye–Waller factors persist).

After another 10 min of heating (20 min total), a significant change in the EXAFS envelope occurs with an associated change in the Fourier transform and a significant increase in the product yield/reactant loss. The best fit to the data now consists of a model containing two carbon atoms at 2.00 Å and two bromine atoms at 2.42 Å. A possible explanation for this is that the catalyst has now formed a new dimeric species containing bridging bromide (reaction (viii), Scheme 2). In the scheme we propose an equilibrium between the dimeric species (**VI**) and the oxidative-addition product (**I**). A closely related mechanistic model was already postulated by Evans et al.[15] in which a dimeric species acts as the starting catalyst. The formation of a dimeric species is also consistent with the reaction profile and the model postulated by De Vries, in which the species involved in the actual catalytic cycle are monomeric and dimeric species and *not* soluble palladium colloids. This hypothesis is also borne out by further EXAFS spectra taken after total heating times of 30 and 50 min, for which the same dibromide model can be fitted successfully to the EXAFS data and high conversion is shown by the reaction profile/yield plot.

To confirm whether oxidative addition had occurred when a temperature of 353 K was reached, a supplementary experiment was conducted with precatalyst complex **2d**, an analogue of **2c** in which Br^- has been replaced by $CF_3SO_3^-$. The occurrence of oxidative addition could easily be proved since the light oxygen scatterer associated with the triflate ion would be substituted by the heavier scatterer Br. When the reaction sequence described above was carried out it was found that a model consisting of only mainly light scatterers gave the best fit to both the k^1 and k^3 data at room temperature (Figure 4, Table 4 in the Supporting Information). However, a small percentage of Br in the model (Br coordination number of about 0.3) was found to improve the *R* factor significantly, that is, even at room temperature some oxidative addition may occur. However, after a temperature of 353 K was reached, the best fit to the data also contained a heavier scatterer, which was best fitted to one bromine atom, which suggests that oxidative addition had taken place. The final model to the 353 K experimental data fitted very well to the main experimental data collected for the precatalyst **2c** (Figure 2, Table 2 in the Supporting Information) with a $N_{pyridine}$–Pd interaction persistent at least until a temperature of 353 K. Finally, analysis of the catalytic solution after heating to 403 K indicated loss of the Pd–$N_{pyridine}$ interaction, but the stability of the Pd–NHC interaction is demonstrated by the significance of the fitting of two nitrogen atoms at 2.84 Å. Therefore from this experiment it can be concluded that oxidative addition is an early step in the reaction mechanism and does, as expected, occur by a temperature of 353 K. However, it is unclear exactly how the oxidative addition mechanism operates, as there is no indication of Pd^0 formation either in the metallic form or as a metal complex (such as the species formed in reaction (v), Scheme 2), and the carbene ligand appears to be present in the 293/353/403 K spectra (as indicated by the two short Pd–C distances of 2.00 Å). The reductive elimination of methylimidazolium[16] as a possible step to Pd^0 formation is therefore an unlikely pathway.

The following conclusions can be drawn from the above-discussed dilute EXAFS data: 1) The Pd–NHC functionality in the catalyst is stable in both catalytic and non-catalytic

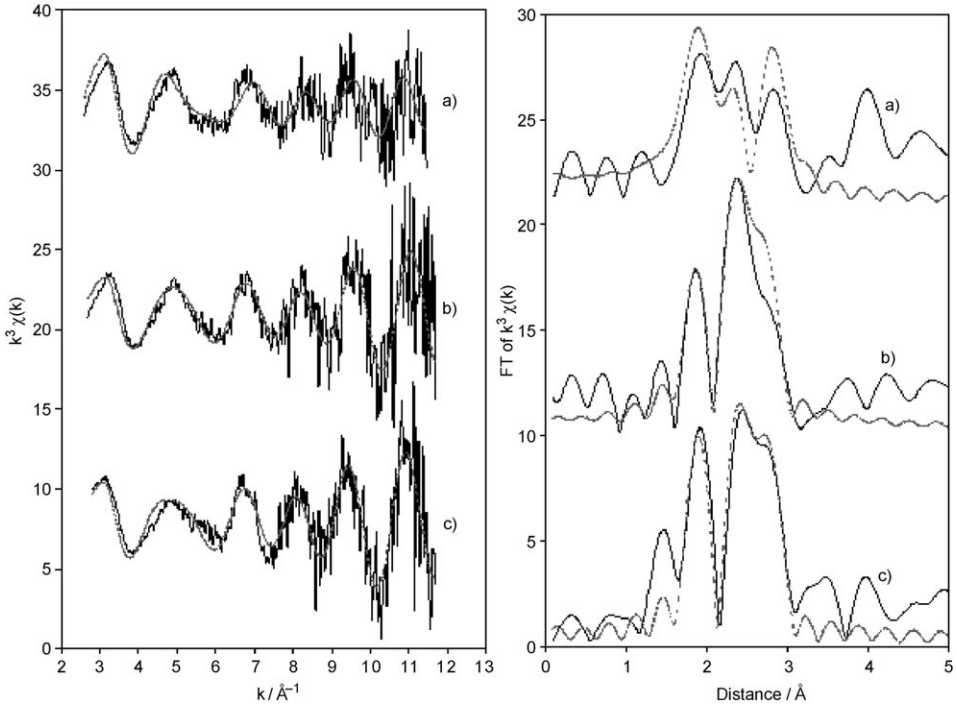

Figure 4. Pd K-edge k^3-weighted EXAFS and Fourier transform, phase-shift-corrected for carbon, of a Pd carbene triflate catalyst (**2d**, Scheme 1) during the Mizoroki–Heck reaction (2 mM Pd) after heating to a) 293 K, b) 353 K and c) 403 K. Black and grey lines represent the experimental and theoretical fits derived from spherical wave analysis in EXCURV98 respectively.

solution. There is good evidence that oxidative addition is the first stage in this reaction and occurs by a temperature of 353 K. However, from our study we cannot suggest which Pd^0 species is formed prior to oxidative addition. Reductive elimination of 2-methylimidazolium from **2c** can be ruled out, as there is always evidence for coordinated NHC at Pd. The possibility of partial involvement of reversible methyl- or phenylimidazolium formation is also highly unlikely since it would require C–C bond cleavage, which has not been reported for relevant metal complexes.

2) On further heating, two important features are detected: Firstly, the loss of $N_{pyridine}$–Pd coordination by 403 K in both **2c** and **2d** could point to a mechanism by which olefin coordination can take place and suggests that, at a certain stage/temperature in the reaction, the pyridyl group becomes highly labile and dissociates from the palladium centre. At no stage of the reaction was there any observable loss of Br, and this provides indirect evidence that coordination of the olefin proceeds via $N_{pyridine}$ and not Br loss. Secondly, the detection (and disappearance) of a small amount of Pd–Pd distances suggests the possible presence of palladium dimers and trimers or soluble Pd colloids stabilised by the NHC ligand. However, it is proposed that these are not the active catalytic species but form monomeric and dimeric species which are involved in the actual catalytic cycle.

3) Finally, EXAFS analysis suggests that dibromine-bridged dimeric species are formed when the conversion to the product is at its maximum; this further evidence in support of monomeric and dimeric species, which are likely to be catalytically active.

In view of these findings, the activity difference observed for **1c** and **2c** may be due to different formation rates of species of type **I** due to the structural differences of the chelating ligand. Complex **1c** with a six-membered chelate ring may undergo pyridine dissociation/oxidative addition faster than the more robust and stable **2c**.

The EXAFS data collected do not help us understand the reactivity differences observed with phosphine-functionalised NHC ligands. Future work is aimed at clarifying these subtle differences, which in the long term may lead to the development of more active catalysts.

Experimental Section

Instrumentation and materials: All reactions were carried out under inert atmosphere. Gas chromatograms were obtained on a Varian 3400GC equipped with a Varian 8100 autosampler, flame-ionisation detector. The column used was Phase DBWAX from J & W Scientific. Complexes **1**–**5** were prepared as previously described.[6a,7a,8,9] Complex **2d** has not been reported before and was prepared by mixing **2c** with an equivalent amount of silver trifluoromethanesulfonate, stirring at room temperature for 24 h, removing the precipitated AgBr by filtration through Celite and evaporating the organic phase to dryness. The off-white product **2d** was formulated as Pd(ligand)-(CH_3)(Br) based on satisfactory analytical and spectroscopic data. All solvents used in the catalytic reactions were dried, distilled and stored over 4 Å molecular sieves under N_2 in sealed glass vessels. All other materials were obtained from commercial suppliers and used without further purification.

General procedure for the Mizoroki–Heck reaction: A 50-mL ampoule equipped with a Young valve was charged with the corresponding aryl halide, alkyl acrylate, base, diethylene glycol dibutyl ether (500 μL, internal standard) and solvent (5 mL). A quantity of standard solution of the catalyst in the same solvent was added to the reaction mixture, and the whole was heated to the specified reaction temperature. After the desired time the reaction mixture was rapidly cooled to room temperature and quenched with water (2 mL) and dichloromethane (5 mL). The organic layer was analysed by gas chromatography. The data reported in Tables 1 and 2 are the average of two separate runs, which typically agree within ±2%.

EXAFS measurements: X-ray absorption spectra were recorded on the undulator beamline ID26 of the European Synchrotron Radiation Facility based in Grenoble, France (operating with an average current of ca. 200 mA in a uniform filling mode). A fixed exit Si(220) monochromator was used, providing an energy resolution of ca. 0.8 eV for XANES and 1.6 eV for EXAFS at the Pd K-edge. For all spectra, a metallic Pd reference foil was used to provide an energy calibration for the monochromator. Two Cr mirrors were used for harmonic rejection of the incident X-ray beam. EXAFS data were recorded in standard scanning mode with each scan taking 20 min. The spectra were acquired at room temperature

in fluorescence mode by a solid-state 13-element germanium detector tuned to the $Pd_{K\alpha}$ fluorescence peak. The solution sample (ca. 4 mL) was injected into a custom-built XAS cell (see Supporting Information) constructed from stainless steel. In addition, at the front of the cell, aluminium windows (20 μm thick) were mounted to permit the entrance of X-rays into the sample and allow fluorescence to be collected. This cell was mounted at about 45° to the direction of the incoming beam with the detector at 90° in the horizontal plane to maximise the fluorescence/scatter ratio. In addition, the stainless steel cell was mounted to an FC 64 flange to allow the cell to be positioned inside a six-way cross to provide a vacuum sleeve and thereby prevent any problems caused by formation of ice crystals on the cell windows. Typically, six scans were collected at the Pd K-edge and summed prior to curve fitting. Background-subtracted EXAFS data were obtained by using the programme PAXAS.[17] Spherical wave curve fitting analysis was executed in EXCURV98,[18] using ab initio phase shifts and backscattering amplitudes calculated by using Von-Barth ground state potentials and Hedin–Lundqvist exchange potentials. Fourier transforms of the EXAFS spectra were used to obtain an approximate radial distribution function around the central transition metal atom; the peaks of the FT can be related to shells of surrounding backscattering atoms, which are characterised by atom type, number of atoms in the shell, the absorber–scatterer distance and the Debye–Waller factor, a measure of both the thermal motion between the absorber and scatterer and the static disorder of the absorber–scatterer distances. The k^3-weighted parameters are presented in Table 1 in the Supporting Information. The accuracy of bonded and non-bonded interatomic distances is considered to be 1.4 and 1.6% respectively.[19] Precision in 1st shell coordination numbers is estimated to be about 5–10% and between 10 and 20% for non-bonded shells. The R factor is defined as $(\int[\chi^T-\chi^E]k^3dk/[\chi^E]k^3dk)\times 100\%$ where χ^T and χ^E are the theoretical and experimental EXAFS and k is the photoelectron wave vector.

Acknowledgements

We thank Johnson-Matthey Catalysts for support of part of this project and generous loan of Pd salts, the EPSRC for support (to N.T. and A.A.D.), the staff of the ESRF for their assistance and the Directors for access to the ESRF.

[1] Reviews: a) *Metal-Catalyzed Cross-Coupling Reactions* (Eds.: F. Diederich, P. J. Stang), Wiley-VCH, Weinheim, **1998**; b) *Cross-Coupling Reactions* (Ed.: N. Miyaura), Springer, New York, *Topics Curr. Chem*. **2002**, *219*, 1.

[2] a) R. B. Bedford, *Chem. Commun.* **2003**, 1787; b) A. Zapf, M. Beller, *Chem. Commun.* **2005**, 431; c) A. F. Littke, G. C. Fu, *Angew. Chem.* **2002**, *114*, 4350; *Angew. Chem. Int. Ed.* **2002**, *41*, 4176.

[3] a) N. S. Phan, M. van der Sluys, C. W. Jones, *Adv. Synth. Catal.* **2006**, *348*, 609; b) J. G. de Vries, *Dalton Trans.* **2006**, 421; c) M. Moreno-Manas, L. Pleixtas, *Acc. Chem. Res.* **2003**, *36*, 638.

[4] W. A. Herrmann, M. Elison, J. Fischer, C. Kocher, G. J. R. Artus, *Angew. Chem.* **1995**, *107*, 2602; *Angew. Chem. Int. Ed. Engl.* **1995**, *34*, 2371.

[5] K. Albert, P. Gisdakis, N Rosch, *Organometallics* **1998**, *17*, 1608.

[6] a) N. Tsoureas, A. A. Danopoulos. A. A. D. Tulloch, M. E. Light, *Organometallics* **2003**, *22*, 4750; b) C. Yang, H. M. Lee, S. P. Nolan, *Org. Lett.* **2001**, *3*, 1511.

[7] a) A. A. D. Tulloch, A. A. Danopoulos, R. P. Tooze, S. M. Cafferkey, S. Kleinhenz, M. B. Hursthouse, *Chem. Commun.* **2000**, 1247; b) D. S. McGuiness, K. J. Cavell, *Organometallics* **2000**, *19*, 741.

[8] A. A. Danopoulos, N. T. Tsoureas, S. MacGregor, C. Smith, *Organometallics*, **2007**, *26*, 253.

[9] A. A. D. Tulloch, S. Winston, A. A. Danopoulos, G. Eastham, M. B. Hursthouse, *Dalton Trans.* **2003**, 699.

[10] J. Evans, W. Levason, R. J. Perry, *J. Chem. Soc. Dalton Trans.* **1990**, 3691.

[11] *Principles, Applications and Techniques of EXAFS, SEAXFS and XANES*, (Eds.: D. C. Koningsberger, R. Prins), Wiley, New York, **1991**.

[12] a) J. M. Vila, M. Gayoso, M. T. Pereira, A. Romar, J. J. Fernandez, M. Thornton-Pett, *J. Organomet. Chem.* **1991**, *401*, 385; b) J. Barro, J. Granell, D. Sainz, J. Sales, *J. Organomet. Chem.* **1993**, *456*, 147; c) A. Crispini, M. Ghedini, F. Neve, *J. Organomet. Chem.* **1993**, *448*, 241; d) N. Gul, J. H. Nelson, *Organometallics* **2000**, *19*, 91.

[13] a) C. Tubaro, A. Biffis, C. Gonzato, M. Zecca, M. Basato, *J. Mol. Catal. A* **2006**, *248*, 93; b) M. Tromp, J. R. A. Sietsma, J. A. van Bokhoven, G. P. F. van Strijdonck, P. W. N. M. van Leeuwen, D. C. Koningsberger, *Chem. Commun.* **2003**, 128.

[14] A. Jentys, *Phys. Chem. Chem. Phys.* **1999**, *1*, 4059.

[15] J. Evans, L. O'Neill, V. L. Kambhampati, G. Rayner, S. Turin, A. Genge, A. J. Dent, T. Neisius, *J. Chem. Soc. Dalton Trans.* **2002**, *10*, 2207.

[16] D. S. McGuiness, N. Saendig, B. F. Yates, K. J. Cavell, *J. Am. Chem. Soc.* **2001**, *123*, 4029.

[17] N. Binsted, PAXAS Programme for the analysis of X-ray absorption spectra, University of Southampton, **1988**.

[18] a) S. J. Gurman, N. Binsted, I. Ross, *J. Phys. C: Solid State Phys.* **1984**, *17*, 143; S. J. Gurman, N. Binsted, I. Ross, *J. Phys. C: Solid State Phys.* **1986**, *19*, 1845; b) N. Binsted, EXCURV98, CCLRC Daresbury Laboratory computer programme, **1998**.

[19] a) J. M. Corker, J. Evans, *J. Chem. Soc. Chem. Commun.*, **1994**, 1027; b) J. M. Corker, J. Evans, H. Leach, W. Levason, *J. Chem. Soc. Chem. Commun.* **1989**, 181.

Received: September 5, 2006
Revised: November 24, 2006
Published online: February 16, 2007

